J Mater Sci (2008) 43:7264–7272
DOI 10.1007/s10853-008-2870-0

ULTRAFINE-GRAINED MATERIALS

Stabilization of nanocrystalline grain sizes by solute additions

C. C. Koch · R. O. Scattergood · K. A. Darling · J. E. Semones

Received: 4 February 2008 / Accepted: 8 July 2008 / Published online: 26 July 2008

Abstract This paper will review the grain growth in nanocrystalline materials with emphasis on the grain size stabilization that can result from solute additions. The grain growth in nominally pure nanocrystalline metals will be presented followed by descriptions of the stabilization of nanocrystalline grain sizes by kinetic approaches and thermodynamic strategies. The descriptions of nanocrystalline grain size by solute additions will be taken from the literature as well as from recent research in the authors' laboratory. Examples of kinetic stabilization, which involves reduction of the grain boundary mobility, include second phase drag, solute drag, chemical ordering, and grain size stabilization. The thermodynamic stabilization, which is due to the lowering of the specific grain boundary energy by solute segregation to the grain boundaries, will be described for systems including Pd–Zr, Fe–Zr, Ni–W, Ni–P, and Co–P. Recrystallization during grain growth will be presented for the Ti–N system. Finally, a summary of alloys where nanocrystalline grain sizes can be maintained at annealing temperatures close to the melting point will be presented.

Introduction

Knowledge of the thermal stability of nanocrystalline materials is important for both technological and scientific reasons. From a technological point of view, the thermal stability is important for consolidation of nanocrystalline particulates without coarsening the microstructure. That is, many methods for synthesis of nanocrystalline materials result in particulate products which must be consolidated into bulk form. Since most consolidation processes involve both heat and pressure, the temperature stability of the nanoscale microstructure is always at risk. The goal of particulate consolidation is to attain essentially 100% theoretical density and good particulate bonding while preventing or minimizing grain growth of the nanocrystalline grains.

Understanding the scientific nature of stability, grain growth of nanocrystalline microstructures is a criterion for allowing strategies for minimizing grain growth to be developed. A basic scientific question with regard to nanocrystalline materials is whether their behavior involves "new physics" or is simply the expected grain size dependent behavior extrapolated to nanocrystalline grain sizes. Thermal stability is an important phenomenon to be addressed in this regard. The thermal stability in a broader sense involves not only the stability of the grain structure, that is, the microstructure, but also the stability of the structure of the grain boundaries in nanocrystalline materials. A number of investigations on the thermal stability of nanocrystalline materials have been conducted. Grain growth in nanocrystalline materials has been reviewed by Suryanarayana [1], Weissmuller [2], and Malow and Koch [3].

In spite of the high driving force for grain growth and the observation of grain growth, at least abnormal grain growth, even at very low homologous temperatures, significant stabilization of nanocrystalline grain structures has been observed in many materials. The one common feature of such materials is that they are multi-component, that is, either alloys or contain impurities. There are two basic ways in which grain growth can be reduced. The first is the *kinetic approach* in which the grain boundaries are pinned

C. C. Koch (✉) · R. O. Scattergood · K. A. Darling · J. E. Semones
Materials Science and Engineering Department, North Carolina State University, Raleigh, NC 27695, USA
e-mail: carl_koch@ncsu.edu

in various ways to decrease grain boundary mobility. The second is the *thermodynamic approach* in which the driving force for grain growth is lowered by reducing the grain boundary energy.

In the kinetic approach the grain boundary mobility is reduced by various possible mechanisms. These include porosity drag [4], second phase drag [5], solute drag [6], chemical ordering [7], and grain size stabilization [8]. The thermodynamic approach depends upon the reduction of the grain boundary energy by solute segregation. Since the driving force for grain growth is directly proportional to the grain boundary energy, reducing the grain boundary energy should minimize grain growth. Addition of solute atoms that segregate to the grain boundaries will affect the grain boundary energy. This concept has been modeled by Weissmuller [9, 10], Kirchheim [11], Liu and Kirchheim [12], and Millett et al. [13]. The grain size at the metastable thermodynamic equilibrium was found in their analysis to be determined by the grain boundary energy, the enthalpy change of grain boundary segregation, and the solute excess of an equivalent grain boundary monolayer at saturation. Good agreement for these predictions of the temperature dependence of the metastable grain size was obtained for $Pd_{100-x}Zr_x$ alloys [12]. The thermodynamic approach to grain size stabilization by segregation of solute, impurity atoms to the grain boundaries appears to be an effective method for stabilization of nanocrystalline grain size.

This paper will review the grain growth in nanocrystalline materials. First the grain growth of nominally pure nanocrystalline metals will be described. This will be followed by discussions of the stabilization of nanocrystalline grain sizes by kinetic approaches and by thermodynamic strategies. The recent dramatic decrease in grain size by recrystallization phenomena will be presented. Finally, a summary of examples of extreme stabilization of nanocrystalline grain structures at temperatures near the material's melting point will be given. Recent work from the authors' laboratory will be emphasized along with results from the literature.

Grain growth in pure nanocrystalline metals

Significant grain growth, that is, doubling of the initial nanocrystalline grain size in 24 hours, has been observed at room temperature in a number of pure, relatively low melting temperature elements such as Sn, Pb, Al, and Mg [14]. Because of the large amount of grain boundary enthalpy stored in the large grain boundary area in nanocrystalline materials, a high driving force for grain growth is expected. Günther et al. [15] studied grain growth in pure Cu, Ag, and Pd and found grain growth occurring at much lower temperatures than those observed for recrystallization of the elements after heavy cold deformation. In fact, grain growth in Cu and Pd was observed even at room temperature. This is particularly dramatic for Pd which has a high melting temperature of 1,552 °C such that room temperature is only 0.16 of the melting temperature—a very low homologous temperature. In all these cases the grain growth was observed to be abnormal. That is, a few grains grew to micron sizes while most grains remained nanoscale. Gertsman and Birringer [16] studied abnormal grain growth in nanocrystalline Cu prepared by the inert gas condensation method with bulk densities of 93%, 96%, and 97%. After holding the samples for times of more than one month at room temperature, abnormal grain growth was observed in all samples. The abnormally coarse grains exhibited a range of sizes, most were <1 μm, but some were >2 μm. The nanocrystalline grains surrounding the coarser grains were about 10–50 nm in size. However, the coarser-grained regions only represented a few percent of the sample volume, with the nanocrystalline grains remaining stable in most of the samples. The growth rate for the average grain size, determined by X-ray diffraction line broadening analysis, was larger for the samples with the higher average densities, implying that porosity was hindering grain boundary migration. The general explanation given for abnormal grain growth is an inhomogeneous structure for the as-processed samples such that grain growth inhibitors such as pores, impurities, or even grain boundary structure are not evenly distributed and rapid grain growth can occur where such inhibitors are absent due to the large driving force and high grain boundary mobility in these regions.

The grain growth in nominally pure elemental metals typically pushes the average grain size to above the nanoscale, that is, greater than 100 nm at annealing temperatures less than 0.5 of the melting temperature. This is illustrated in Fig. 1 for nominally pure Pd [17], Fe [18, 19], Cu [20], and Ni [21].

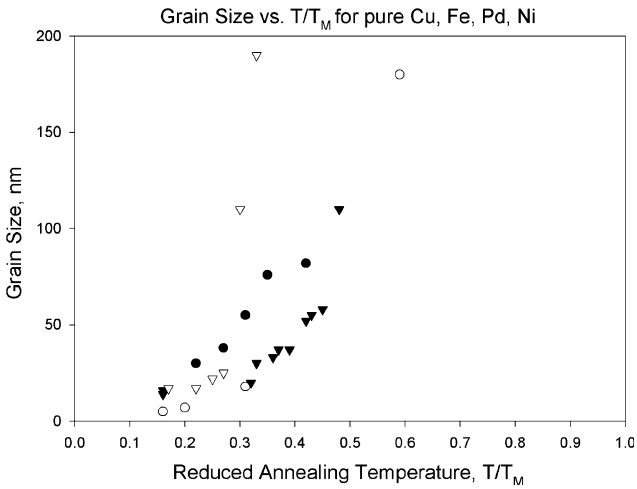

Fig. 1 Grain size versus reduced annealing temperature (T/T_M) for pure Cu ● [20], Fe ▼ [18, 19], Pd ○ [20], Ni ▽ [21]

A general expression for grain growth in terms of the velocity of the boundary can be given as: $v \sim M\frac{\gamma}{r}$ where M is the grain boundary mobility, γ is the specific grain boundary energy, and r is the average grain radius [22, 23].

Examples of kinetic stabilization of nanocrystalline grain sizes

In the kinetic approach the grain boundary mobility is reduced by various possible mechanisms. We will focus on those that involve the action of solute atoms.

Second phase drag: There have been a number of examples of grain boundary pinning in nanocrystalline materials by the presence of small second phase particles—the Zener drag mechanism [24]. The expression for the pinning pressure exerted on the grain boundary by small particles is:

$$P_Z = \frac{3F\gamma}{2r}$$

where P_Z is the pinning pressure exerted by the particles on unit area of the boundary, F is the volume fraction of randomly distributed spherical particles of radius r, and γ is the specific grain boundary energy. It is clear that a high volume of small particles is desirable to increase the pinning pressure and thus to impede grain boundary mobility. The stabilization in 5 nm grain size Ni–P alloys, which were produced by electrodeposition, did not take effect until after an increase of the grain size by a factor of 2–3 [5]. The solid solution of the Ni—1.2% P alloy did not measurably grow and was stable as a solid solution up to an annealing temperature of 473 K. For annealing temperatures of 523 and 623 K, the grain size initially increased by a factor of 2–3, before the grain size stabilized, which coincided with the precipitation of a second phase, Ni_3P. Although other retarding effects in reducing the grain boundary mobility are considered (solute drag), the pinning of the grain boundaries by Ni_3P as the second phase was believed to be the major factor of the grain size stabilization at 573 and 623 K. The same effect was found for electroplated 10 nm Ni with an addition of 0.12 wt.% S [25], where it was attributed to the formation of nickel sulfide precipitates. Another example of nanocrystalline grain size stabilization by second phase particles is the work of Perez et al. [26]. The authors studied the thermal stability of cryomilled Fe-10 wt.% Al and found that a grain size of about 20 nm was maintained after annealing to about 600 °C, and even after annealing at 1,100 °C the grain size only grew to about 50 nm. This excellent grain size stability was attributed to the presence of nanoscale Al_2O_3 and AlN dispersoids. Another example of small particle induced grain size stabilization is for an Al—base alloy by Shaw et al. [27]. An $Al_{93}Fe_3Cr_2Ti_2$ alloy was prepared by mechanical alloying. The as-milled alloy was a solid solution of Al. After annealing at various temperatures the internal strain was released, intermetallic compound particles precipitated, and there was some grain growth. The precipitation of a variety of intermetallics with Cr, Fe, or Ti was followed with several analytical techniques. There was essentially no grain growth at temperatures up to about 300 °C with the grain size distribution from TEM being about 6–45 nm. Even after heating to 450 °C ($0.77T_m$), the grain size distribution was still nanoscale, that is, from 20–100 nm. The authors believe that the inhibition of grain growth at the lower annealing temperature was due to solute drag on the grain boundaries, but at the higher temperatures was due to pinning of the boundaries by the nanoscale intermetallic precipitates.

Solute drag: In the case of grain growth in nanocrystalline materials containing solutes or impurities, the segregation of the solute atoms to the grain boundaries may depend upon the grain size. This problem was treated by Michels et al. [6], with several experimental examples given. The equilibrium segregation to grain boundaries can be attained by diffusion of solute atoms through the lattice to the boundaries, or by the entrapment of solute at the boundaries as they move. Since in nanocrystalline materials grain growth usually occurs at temperatures too low for significant lattice diffusion, it is suggested that the latter mechanism is more likely. This mechanism of solute entrapment by moving boundaries was used by Knauth et al. [28] to explain the differences in DSC results for grain growth in nanocrystalline Ni and Ni-1 at.% Si. While grain growth started at about the same temperature in both materials, the growth in the Ni-1 at.% Si alloy slowed dramatically, presumably as the result of entrapment of Si atoms at the grain boundaries and their effect on the boundary mobility. Michels et al. [6] provided additional evidence for solute entrapment in moving grain boundaries for the Pd-19 at.% Zr nanocrystalline alloy. The grain size increased with annealing time at 600 °C from about 5 nm to a saturation value of about 16 nm. At the same time, the solute composition at grain boundaries (determined by lattice parameter measurements) increased from 19% Zr to about 27% Zr.

Chemical ordering: Reduced grain growth has been observed for ordered nanocrystalline intermetallic compounds. For example, the thermal stability of Fe_3Si with and without 5% Nb additions was studied by Gao and Fultz, [7, 29]. The mechanical alloying of the alloys resulted in disordered products with an initial grain size <10 nm for the $(Fe_3Si)_{95}Nb_5$ alloy. Three different processes were identified to occur simultaneously, when the samples were annealed isothermally at temperatures between 350 and 500 °C. In an initial stage, the grain growth is thought to take place

uninhibited. After that, the segregation of Nb to the grain boundaries, occurring at the same time as grain growth, is believed to provide the alloy with considerable stabilization of the grain size over the Fe_3Si alloy. The other process that is thought to inhibit the grain growth is the chemical ordering process to form the DO_3 structure of the ordered Fe_3Si, which did not happen homogeneously, but rather by nucleation and growth. It was also suggested that the segregation of the Nb atoms to the grain boundaries and the ordering process are interdependent. The ordering process is simplified by the diffusion of the Nb atoms out of the grains, because the ordering is easier in Fe_3Si compared to $(Fe_3Si)_{95}Nb_5$. Bansal et al. [30] replaced the Nb additions with Mn, which is not expected to segregate to the grain boundaries since it replaces Fe atoms on specific sites in the ordered DO_3 structure. The ordering kinetics of the alloy with Mn were found to be accelerated compared to the binary alloy. At the same time, the grain growth was slowed down, which was linked to the enhanced ordering kinetics. The authors suspected decreasing grain boundary mobility with an increase of the ordering parameter of the alloy upon annealing. They conclude that once ordering had taken place, the grain growth is inhibited, hypothesizing that the grain boundary mobility is decreased in the ordered compound. This may be due to the fact that diffusion is typically slower in ordered structures compared to their disordered counterparts.

Grain size stabilization: Grain size dependent stabilization of a nanocrystalline microstructure has been experimentally observed [31, 32] and more recently predicted by theoretical models. Estrin et al. [33] suggest that at small grain sizes the rate-controlling step for boundary migration is transport of excess volume, located at the grain boundaries, away from the moving boundaries. In computer simulations of Upmanyu et al. [34] it was shown that the excess volume released from the boundaries during grain growth is incorporated into the crystalline lattice in the form of vacancies. This increase in the non-equilibrium vacancy concentration gives rise to an increase in free energy that counteracts the decrease in free energy associated with the reduction in grain boundary area during grain growth. These theories lead to a prediction of a linear dependence of the grain size on annealing time when the grain size is below some critical value. Linear growth kinetics are in agreement with experimental work of Krill et al. [32] on nanocrystalline Fe.

Examples of thermodynamic stabilization nanocrystalline materials

Since the driving force for grain growth is directly proportional to the grain boundary energy, reducing the grain boundary energy should minimize grain growth. Addition of solute atoms that segregate to the grain boundaries will affect the grain boundary energy. The energy varies with the overall solute concentration, c_s, according to the Gibbs (adsorption) equation:

$$\partial \gamma_b / \partial \ln c_s = -RT\Gamma_s$$

where T is the temperature, γ_b is the specific interfacial energy, c_s is the solute concentration, and Γ_s is the interfacial excess of the solute atoms. For grain boundary segregation of solute, $\Gamma_s > 0$ and therefore γ_b will decrease with increasing c_s. Hondros and Seah [35] reported a decrease in γ_b for several binary alloys. The greater the difference in atomic size is between the solute and solvent atoms, more negative is the initial slope of the γ_b vs. c_s curves. This suggests that elastic strain energy induces solute segregation to grain boundaries [35]. Based on this, solute additions to induce the lowering of the grain boundary energy and stabilize the grain size against coarsening should be much larger, or smaller, than the host atom. Weissmuller [9, 10] has applied these ideas to nanocrystalline materials and quantified the effects of segregation on grain size stability. He predicts that for alloy systems with a large heat of segregation, the nanocrystalline alloy is in a metastable state for a particular grain size which decreases with increasing concentration of the solute element. In the metastable state, the specific grain boundary energy is zero. Subsequently, Kirchheim [11] and Liu and Kirchheim, [12] have extended these concepts and have compared their predictions with experimental data. The grain size at the metastable thermodynamic equilibrium was found in their analysis to be determined by the grain boundary energy, the enthalpy change of grain boundary segregation, and the solute excess of an equivalent grain boundary monolayer at saturation. Good agreement for these predictions of the temperature dependence of the metastable grain size was obtained for Pd_{100-x} Zr_x alloys [12]. Other experimental studies of the stabilization of nanocrystalline grain size by the lowering of the grain boundary energy due to solute segregation have been reported for Ni–P alloys [36], RuAl with Fe impurities [37], Nb–Cu alloys [38], Ti–Cu alloys [39], Y–Fe alloys [40], and TiO_2 with Ca [41]. In those alloy systems that are metastable solid solutions due to non-equilibrium processing, the grain size stabilization appears to be dominated by the segregation of solute to the grain boundaries and the lowering of the grain boundary energy at lower annealing temperatures. At higher temperatures when precipitation of solute-rich phases can occur, dramatic increases in grain growth are typically observed showing that the loss of grain boundary segregation is more important than any stabilizing effect of the second phases.

An alloy system which has been studied extensively is nanocrystalline Pd with Zr additions [42–44]. The results have been summarized by Krill et al. [45]. The latter authors derive an expression for the grain boundary energy as affected by solute segregation as follows:

$\gamma = \gamma_o - \Delta H^{seg} (\frac{n_B^{seg}}{A})$, where γ_o = the specific grain boundary energy of the pure element, ΔH^{seg} = the enthalpy of segregation of B solute atoms to the grain boundary, n_B^{seg} = number of moles of B solute atoms segregated to the grain boundary phase, and A = total grain boundary area. Insertion of typical numbers for these quantities gives a value for $\gamma \sim 0$ when $\Delta H^{seg} = 25$ kJ/mol or more. The segregation enthalpy of Zr in Pd is estimated to be 31 kJ/mol [46]. However, the solid solubility of Zr in Pd at 600 °C is 12 at.% and increases up to 17 at.% at the peritectic temperature [47]. In their initial studies of the Pd–Zr alloys, Krill and co-workers [42, 43] found that ball milling induced metastable solid solutions up to 20 at.% Zr. At concentrations of 21 at.% Zr and higher, the intermetallic Pd_3Zr phase formed. The lattice parameters of the metastable Pd–Zr alloys (>12 at.% Zr) showed an approximately linear increase with Zr concentration [42]. The lattice parameters decreased on annealing at 500 °C which the authors attributed to the segregation of Zr atoms to the grain boundaries. Annealing for two hours at 500 °C increased the grain sizes, but the increase was less as Zr concentration increased. The approximately linear decrease in grain size with at.% Zr for the annealed samples has a higher slope than that of the as-milled alloys. The authors subsequently found [45] that raising the Zr concentration increased the onset temperature for significant grain growth and it suppressed the rate at which coarsening progressed. They attributed these effects to the segregation of Zr atoms to the grain boundaries. This segregation may lead either to kinetic stabilization by solute drag on the boundaries or to thermodynamic stabilization by lowering the grain boundary energy, or a combination of the two. From their X-ray data for grain size and lattice parameter changes with Zr concentration and annealing temperatures up to 1,125 °C, the authors [45] estimated the areal density of Zr atoms segregated to the grain boundaries, which increased with annealing temperature, and the specific grain boundary energy, which decreased with annealing temperature. The authors suggest that while the enhanced stabilization at low and moderate temperatures may be partly due to solute drag, only the thermodynamic stabilization can provide a credible explanation for the enhanced stability at high temperatures. Subsequently, annealing of the 15, 19, and 20 at.% Zr nanocrystalline alloys was conducted at 1,500 °C, a temperature ~95% of the melting temperatures. The grain size of the 15 at.% Zr sample grew slightly, while those of the 19 and 20 at.% Zr samples remained approximately at the values obtained at 1,125 °C. The grain sizes vs. annealing temperature, normalized by the melting temperature, are plotted in Fig. 2 for these alloys.

Recently, Darling et al. [48] studied the influence of solute Zr atoms on the stability of the grain size of nanocrystalline Fe. Zr was selected for this study of potential thermodynamic stabilization because Zr in Fe has a large positive elastic enthalpy of +92 kJ/mol and a large negative enthalpy of mixing of −118 kJ/mol [46]. The large elastic enthalpy indicates that these alloys should favor grain boundary segregation of solute atoms. The large negative enthalpy of mixing suggests that once segregates form on a grain boundary, the solute atoms should resist the formation of the several Fe–Zr intermetallic phases indicated by the phase diagram [49]. These thermodynamic data suggest that nanocrystalline Fe(Zr) should be an ideal system for a study of thermodynamic grain size stabilization. The nanocrystalline Fe(Zr) alloys were prepared by ball milling of the elemental powders at compositions of 1, 4, 7, and 10 atomic percent Zr. Milling was carried out for 20 hours at room temperature. The milled powders, after characterization for grain size, were subsequently heat treated at 340, 500, 700, 850, 1,000, 1,150, and 1,375 °C for 60 minutes in an Ar/2%H atmosphere. The as-milled powders showed metastable solid solubility for all the alloys (1–10 at.% Zr) studied. On annealing, precipitation of Fe_2Zr was observed at 1,000 °C for the 7 at.% Zr alloy, and at 500 °C for the 10 at.% Zr alloy. The 1 and 4 at.% Zr alloys maintained complete solubility (from X-ray diffraction measurements) at all annealing temperatures and times including 1,375 °C for one hour. On isothermal annealing it was found that the grain size grew initially, and then stagnated with further annealing time. At the same time the lattice parameter of the Fe (Zr) solid solution decreased

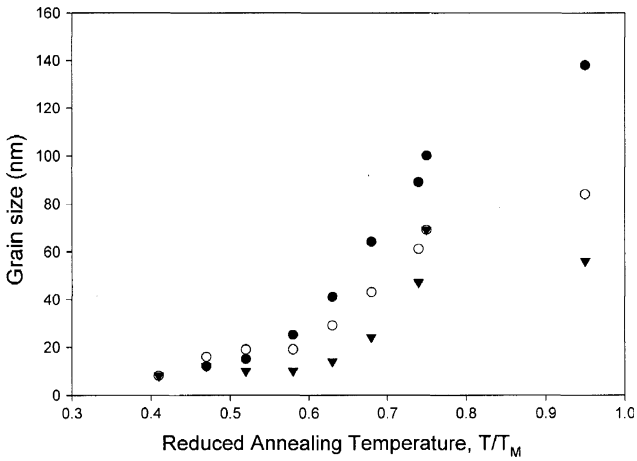

Fig. 2 Grain size versus reduced annealing temperature (T/T_M) for nanocrystalline Pd–Zr alloys. Pd-15 at.% Zr ●; Pd-19 at.% Zr ○; Pd-20 at.% Zr ▼ [data from ref. 47]

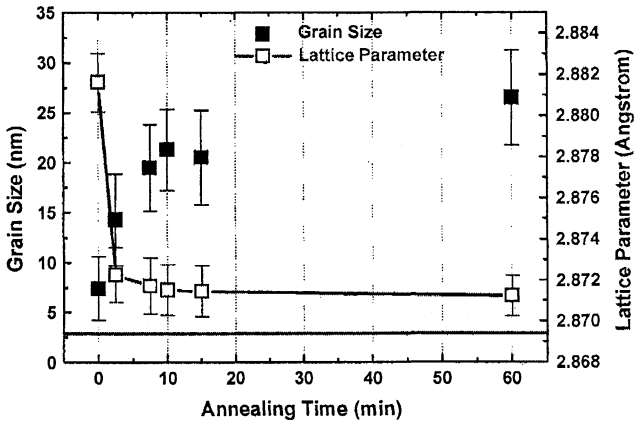

Fig. 3 Change in lattice parameter and grain size for Fe-4 at.% Zr annealed at 800 °C [50]

rapidly toward that of pure Fe. These results are illustrated in Fig. 3 for the Fe-4 at.% Zr alloy annealed at 800 °C. The drop in lattice parameter on annealing must mean that Zr solute atoms leave the Fe lattice and segregate to the grain boundaries. However, energy dispersive spectroscopy (EDS) showed that some Zr segregation to the particle surfaces also occurred. Therefore, a precise analysis of the amount of Zr segregated to the grain boundaries was not possible. The grain size versus T/T_M, where T is the annealing temperature and T_M is the liquidus temperature of the alloy, is given in Fig. 4 for nanocrystalline Fe, Fe-10 at.% Cr, Fe-1 at.% Zr, and Fe-4 at.% Zr. It is evident that the grain size of pure nanocrystalline Fe grows to greater than 100 nm at temperatures below about 0.5 T/T_M. The addition of 10 wt.% Cr to nanocrystalline Fe has little effect of the grain size stabilization, as might be expected since Cr has a similar atomic size to Fe and the elastic enthalpy is $\sim$ 0 such that complete solubility is observed and little

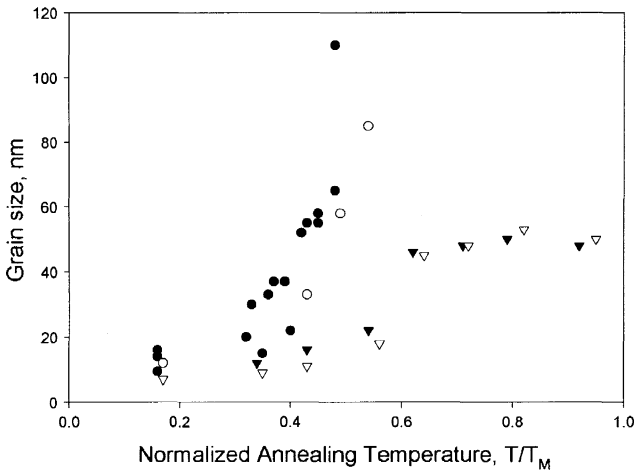

Fig. 4 Grain size versus reduced annealing temperature (T/T_M) for Fe ● [18, 19]; Fe-10 wt.% Cr ○; Fe-1 at.% Zr ▼ [50]; Fe-4 at.% Zr ▽ [50]

grain boundary segregation is likely. However, both the 1 and 4 at.% Zr additions to nanocrystalline Fe resulted in significant stabilization of the grains with little difference between the 1 and 4 at.% Zr alloys. There is very little grain growth in the Fe-1 at.% Zr nanocrystalline alloy until about 0.5 T/T_M. However, this grain growth stops at a temperature between 0.6 and 0.7 T/T_M and, remarkably, stays about constant up to temperatures near the melting point, i.e., 92–95% of T_M. Based on a simple estimate, and the observation of surface segregation and lattice parameter change in the Fe-1 at.% Zr alloy, it appears that stabilization can be achieved with less than a monolayer of Zr on the grain boundaries. Increasing the solute content to 4 at.% Zr produced no additional stabilization and no intermediate phases.

A very detailed study of grain boundary segregation has been carried out by Detor and Schuh in nanocrystalline Ni–W alloys made by electrodeposition [50, 51]. The elastic enthalpy for W solute in Ni is estimated to be 60 kJ/mol [45] although there is significant solid solubility of W in Ni of >10 at.% W [52]. From precise lattice parameter measurements as a function of W composition [50] and from atomistic computer simulations [51] and atom-probe tomography [53], it was determined that the segregation tendency for W to grain boundaries in Ni is weak. Segregation energy decreased with W addition from a dilute limit value owing to solute–solute interactions in the grain boundaries. The grain boundary energy decreased with W additions but did not reach zero for any composition or grain size considered. Detor and Schuh [54] have subsequently measured the grain growth in their electrodeposited nanocrystalline Ni–W alloys. The as-deposited grain size was a function of composition, with the smallest grain sizes (3 nm) corresponding to the highest W content (21 at.%) and the largest grain size (70 nm) for the lowest W concentration (6 at.%). The grain size for three Ni–W samples is plotted versus reduced annealing temperature (T/T_M) in Fig. 5. These data were obtained by analysis of X-ray diffraction line broadening. However, TEM studies on these samples showed good agreement with the X-ray data and gave no evidence for abnormal grain growth. While good stabilization compared to pure Ni occurs for these alloys up to about $T/T_M = 0.4$, significant grain growth begins by $T/T_M \sim 0.5$ and the grains grow to above 100 nm (out of the nanoscale regime) by 0.6–0.7. The initial grain sizes of the electrodeposited alloys, and the stabilization, are strong functions of the W concentration. The Ni-21 at.% W alloy with as-deposited grain size of 3 nm is the most stable. It does precipitate the intermetallic compound Ni_4W at the highest annealing temperature of 900 °C. The lower W content alloys maintain the fcc solid solution structure up to this temperature. The grain growth curves for the three alloys shown in Fig. 5 appear to be almost parallel. This

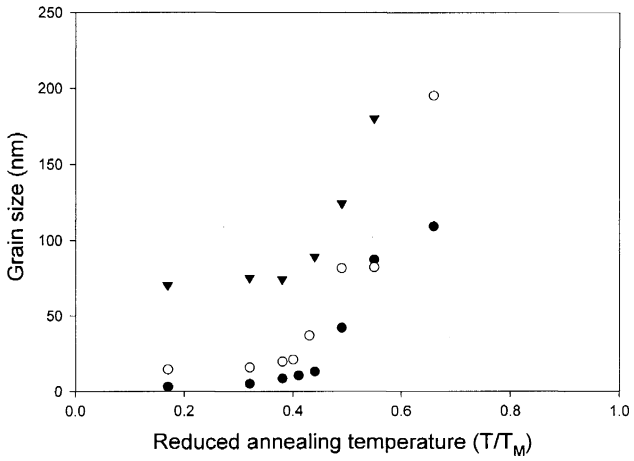

Fig. 5 Grain size versus reduced annealing temperature (T/T_M) for Ni-6 at.% W ▼, Ni-13 at.% W ○, Ni-21 at.% W ●; data from ref. [56]

suggests that the stabilization effectiveness for the various alloys may be similar if they were normalized to the same as-deposited grain size. Whether the stabilization is partially due to solute drag or thermodynamic stabilization is not clear although reduction in grain boundary energy was determined [51].

The dependence of as-deposited grain size on composition in nanocrystalline alloys prepared by electrodeposition had been clearly noted in Ni–P alloys [36]. The authors studied the microstructures of Ni–P alloys including the grain boundary segregation with tomographic atom probe analysis. The composition dependence of the grain size was explained by assuming a metastable grain boundary phase, of 15 at.% P, and thickness of 0.8 nm and using a mass balance calculation. It was possible to predict the grain size—P concentration relationship in as-deposited and annealed alloys. For low P content (less than about 5 at.%) the grain size increased upon annealing, while at the higher concentrations (>10 at.%) there was little difference between the as-deposited and annealed grain size. These were for annealing temperatures around 300 °C which are below the critical temperature where Ni_3P formation starts. At 15 at.% P the samples become amorphous—in a sense, become "all grain boundary." This same approach might also apply to the Ni–W nanocrystalline alloys made by electrodeposition, as discussed above. Whether similar ideas can be applied to nanocrystalline alloys made by other methods such as ball milling is problematic.

Nanocrystalline Co-1.1 at.% P was prepared by pulsed electrodeposition [55]. Its thermal stability was studied by a variety of characterization methods including tomographic atom probe analysis. The thermal stability of the alloy at temperatures below about 733 K was attributed to the reduction in grain boundary energy due to segregation of P to the grain boundaries. At temperatures between 673 and 733 K, the allotropic phase transformation, hcp–Co to fcc–Co, occurs and abnormal grain growth is observed. It was suggested that there is a synergistic relationship between the abnormal grain growth and the phase transformation.

Recrystallization during grain growth of nanocrystalline materials

There is one example of the apparent recrystallization of the nanocrystalline grain structure during annealing. That is the work of Sun et al. [56] on nanocrystalline Ti produced by cryomilling. That is, the Ti powder was milled in liquid nitrogen. A fine grain size of about 20 nm was obtained along with the addition of about 2 wt.% nitrogen. The nitrogen was in solid solution in the hcp Ti matrix. The grain size, as determined by X-ray diffraction and checked by TEM, increased up to about 80 nm at 350 °C. At slightly higher annealing temperatures the samples underwent a dramatic recrystallization phenomenon and the average grain size decreased to about 15 nm. Annealing at temperatures up to 720 °C resulted in a small increase in average grain size to about 27 nm. These grain size results are plotted in Fig. 6 versus normalized annealing temperature, T/T_M. The authors attribute the recrystallization reaction to the reordering of the nitrogen atoms in the octahedral interstices in the hcp Ti phase. No annealing was carried out above the temperature where the hcp phase transforms to the bcc structure. It is not clear how general such recrystallization phenomena may be in terms of providing decreased grain sizes in nanocrystalline materials at elevated temperatures. Preliminary results [57] in our laboratory suggest, in fact, that such behavior may be seen in

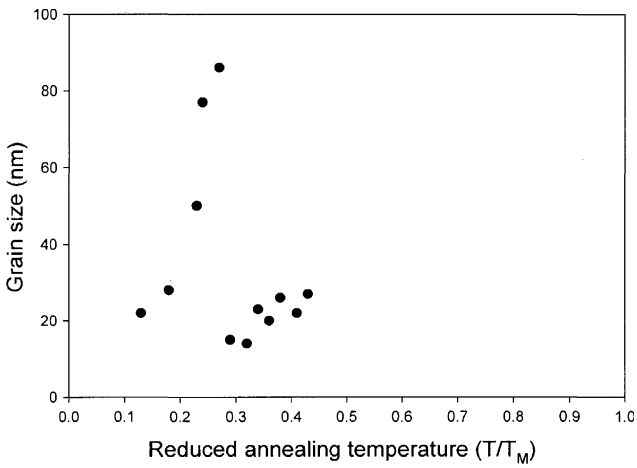

Fig. 6 Grain size versus reduced annealing temperature (T/T_M) for Ti-2 wt.% N; data from ref. [59]

other alloy systems. More research is needed to confirm these results and define the mechanism responsible.

Summary: examples of nanoscale grain size stabilization at high homologous temperatures

We have described the stabilization of nanocrystalline grain sizes to temperatures approaching the melting point of the alloys in the Pd–Zr [45] and Fe–Zr [48] systems. In addition, Botcharova et al. [58] have reported high stability of the nanocrystalline Cu matrix in Cu–Nb alloys. Nanocrystalline Cu and Cu–Nb alloys were prepared by the consolidation of mechanically alloyed powder. The alloys showed a microstructure with a grain size below 50 nm. Cu and Nb have little mutual solid solubility in equilibrium. Previous studies of the ball milling of Cu and Nb powders have suggested that about 3–4 at.% Nb metastable solid solution can be formed in Cu milled at room temperature [59] or up to about 10 at.% Nb in Cu milled at liquid nitrogen temperature [60]. The study of Botcharova et al. [58] did not report the as-milled microstructure, but after consolidation at different temperatures (600, 700, and 800 °C) Nb precipitates were seen in the alloys studied (5, 7, and 10 at.% Nb). On subsequent annealing the Nb particles coarsened significantly while the Cu matrix grain size showed some growth, but remarkable stability. At 1,000 °C, 0.94 of the melting temperature, the Nb precipitates had grown to about 600 nm while the Cu grains for the Cu-10 at.% Nb alloy remained at about 50 nm. No explanations were offered for this behavior.

For the cases of grain size stabilization in the Pd–Zr [47} and Fe–Zr [50} alloys, it seems likely that thermodynamic stabilization mechanisms are important. In fact, Krill et al. state [ref. 47 p. 1140] that "only the thermodynamics of segregation provide a credible explanation for the lack of grain growth at higher temperatures." The case of the Cu–Nb alloys is more complex since there is the presence of the second phase Nb particles along with metastable solid solution of Nb in Cu.

It is now clear that significant stabilization of nanocrystalline grain structures can be achieved up to temperatures near the melting point of the alloys. The detailed mechanisms responsible still require clarification. The intriguing possibility of recrystallization phenomena opening up a wide range of alloys with nanocrystalline grains at high temperatures to make feasible consolidation of particulates is an area deserving of further study.

Acknowledgements The authors wish to thank the National Science Foundation for supporting their research on this topic under grant number DMR-0504286.

References

1. Suryanarayana C (1995) Int Mater Rev 40:41
2. Weissmuller J (1996) Synthesis and processing of nanocrystalline powder. In: Bourell DL (ed) TMS, Warrendale, PA, p 3
3. Malow TR, Koch CC (1996) Synthesis and processing of nanocrystalline powder. In: Bourell DL (ed) TMS, Warrendale, PA, p 33
4. Hofler HJ, Averback RS (1990) Scr Metall Mater 24:2401. doi:10.1016/0956-716X(90)90101-L
5. Boylan K, Osstrander D, Erb U, Palumbo G, Aust KT (1991) Scr Metall Mater 25:2711. doi:10.1016/0956-716X(91)90144-P
6. Michels A, Krill CE, Ehrhardt H, Birringer R, Wu DT (1999) Acta Mater 47:2143. doi:10.1016/S1359-6454(99)00079-8
7. Gao Z, Fultz B (1994) NanoStructured Mater 4:939. doi:10.1016/0965-9773(94)90100-7
8. Krill CE, Helfen L, Michels D, Natter H, Fitch A, Masson O et al (2001) Phys Rev Lett 86:842. doi:10.1103/PhysRevLett.86.842
9. Weissmuller J (1993) NanoStructured Mater 3:261. doi:10.1016/0965-9773(93)90088-S
10. Weissmuller J (1994) J Mater Res 9:4. doi:10.1557/JMR.1994.0004
11. Kirchheim R (2002) Acta Mater 50:413. doi:10.1016/S1359-6454(01)00338-X
12. Liu F, Kirchheim R (2004) Scr Mater 51:521. doi:10.1016/j.scriptamat.2004.05.042
13. Millett PC, Selvam RP, Saxena A (2007) Acta Mater 55:2329. doi:10.1016/j.actamat.2006.11.028
14. Birringer R (1989) Mater Sci Eng A A117:33. doi:10.1016/0921-5093(89)90083-X
15. Gunther B, Kumpmann A, Kunze H-D (1992) Scr Metall Mater 27:833. doi:10.1016/0956-716X(92)90401-Y
16. Gertsman VY, Birringer R (1994) Scr Metall Mater 30:577. doi:10.1016/0956-716X(94)90432-4
17. Sanders PG, Weertman JR, Baker JG, Siegel RW (1993) Scr Metall Mater 29:91. doi:10.1016/0956-716X(93)90260-Y
18. Moelle CH, Fecht HJ (1995) NanoStructured Mater 6:421. doi:10.1016/0965-9773(95)00086-0
19. Michels A, Krill CE, Natter H, Birringer R (1998) Grain growth in polycrystalline materials III. In: Weiland H, Adams BL, Rollett AD (eds) TMS, Warrendale, PA, p 449
20. Lu L, Tao NR, Wang LB, Ding BZ, Lu K (2001) J Appl Phys 89:6408. doi:10.1063/1.1367401
21. Natter H, Schmelzer M, Hempelmann R (1998) J Mater Res 13:1186. doi:10.1557/JMR.1998.0169
22. Humphreys FJ, Hatherly M (1996) Recrystallization and related annealing phenomena, Chapt 9. Elsevier Science Inc, Tarrytown, NY, pp 289–295
23. Krill CE, Ehrhardt H, Birringer R, Metallkd Z (2005) 96:1134
24. Humphreys FJ, Hatherly M (1996) Recrystallization and related annealing phenomena, Chapt 9. Elsevier Science Inc, Tarrytown, NY, p 281
25. El-Sherik AM, Boylan D, Erb U, Palumbo G, Aust KT (1992) Mater Res Soc Symp Proc 238:727
26. Perez RJ, Jiang HG, Dogan CP, Lavernia EJ (1998) Metall Mater Trans A 29A:2469. doi:10.1007/s11661-998-0218-7
27. Shaw L, Luo H, Villegas J, Miracle D (2003) Acta Mater 51:2647. doi:10.1016/S1359-6454(03)00075-2
28. Knauth P, Charai A, Gas P (1993) Scr Metall Mater 28:325. doi:10.1016/0956-716X(93)90436-V
29. Gao Z, Fultz B (1993) NanoStructured Mater 2:231. doi:10.1016/0965-9773(93)90150-A
30. Bansal C, Gao Z, Fultz B (1995) NanoStructured Mater 5:327. doi:10.1016/0965-9773(95)00236-8

31. Lu K (1993) NanoStructured Mater 2:643. doi:10.1016/0965-9773(93)90039-E
32. Krill CE III, Helfen L, Michels D, Natter H, Fitch A, Masson O et al (2001) Phys Rev Lett 86:842. doi:10.1103/PhysRevLett.86.842
33. Estrin Y, Gottstein G, Rabkin E, Shvindlerman LS (2000) Scr Mater 43:141. doi:10.1016/S1359-6462(00)00383-3
34. Upmanyu M, Srolovitz DJ, Shvindlerman LS, Gottstein G (1998) Interface Sci 6:287
35. Hondros ED, Seah MP (1983) Physical metallurgy. In: Cahn RW, Haasen P (eds) 3rd edn. Elsevier Sci Pub BV, Netherlands, p 856
36. Farber B, Cadel E, Menand A, Schmitz G, Kirchheim R (2000) Acta Mater 48:789. doi:10.1016/S1359-6454(99)00397-3
37. Liu KW, Mucklich F (2001) Acta Mater 49:395. doi:10.1016/S1359-6454(00)00340-2
38. Abe YR, Holzer JC, Johnson WL (1992) Mater Res Soc Symp Proc 238:721
39. Abe YR, Johnson WL (1992) Mater Sci Forum 88–90:513
40. Weissmuller J, Krauss W, Haubold T, Birringer R, Gleiter H (1992) NanoStructured Mater 1:439. doi:10.1016/0965-9773(92)90076-A
41. Terwilliger CD, Chiang YM (1995) Acta Mater 43:319
42. Krill CE, Ehrhardt H, Birringer R (1997) Chemistry and physics of nanostructures and related non-equilibrium materials. In: Ma E, Fultz B, Shull R, Morral J, Nash P(eds) TMS, Warrendale, PA, pp 115–124
43. Krill CE, Klein R, Janes S, Birringer R (1995) Mater Sci Forum 179–181:443
44. Shapiro E, Wurschum R, Schaefer H-E, Ehrhardt H, Krill CE, Birringer R (2000) Mater Sci Forum 343–346:726
45. Krill CE, Ehrhardt H, Birringer R, Metallkd R (2005) 96:1134
46. De Boer FR, Boom R, Mattens WCM, Miedema AR, Niessen AK (1988) Cohesion in metals: transition metal alloys. North-Holland, Amsterdam, p 748
47. Okamoto H (ed) (2000) Phase diagrams for binary alloys. ASM International, Metals Park, OH, p 664
48. Darling KA, Chan RN, Wong PZ, Semones JE, Scattergood RO, Koch CC (2008) Scripta Materialia 59:530
49. Okamoto H (ed) (2000) Phase diagrams for binary alloys. ASM International, Metals Park, OH, p 380
50. Detor AJ, Schuh CA (2007) Acta Mater 55:371. doi:10.1016/j.actamat.2006.08.032
51. Detor AJ, Schuh CA (2007) Acta Mater 55:4221. doi:10.1016/j.actamat.2007.03.024
52. Okamoto H (ed) (2000) Phase diagrams for binary alloys. ASM International, Metals Park, OH, p 626
53. Detor AJ, Miller JK, Schuh CA (2006) Philos Mag 86:4459. doi:10.1080/14786430600726749
54. Detor AJ, Schuh CA (2007) J Mater Res 22:3233. doi:10.1557/jmr.2007.0403
55. Choi P, Da Silva M, Klement U, Al-Kassab T, Kirchheim R (2005) Acta Mater 53:4473. doi:10.1016/j.actamat.2005.06.006
56. Sun F, Zuniga A, Rojas P, Lavernia EJ (2006) Metall Mater Trans A 37A:2069. doi:10.1007/BF02586127
57. Darling KA, Semones JE, Scattergood RO, Koch CC (2008) Unpublished research, North Carolina State University
58. Botcharova E, Freudenberger J, Schultz L (2006) Acta Mater 54:3333. doi:10.1016/j.actamat.2006.03.021
59. Benghalem A, Morris DG (1992) Scr Metall Mater 27:739. doi:10.1016/0956-716X(92)90498-4
60. Botcharova E, Freudenberger J, Schultz L (2004) J Alloy Comp 365:157. doi:10.1016/S0925-8388(03)00634-0